Journal of Medical and Biological Engineering (2020) 40:934–942
https://doi.org/10.1007/s40846-020-00573-0

ORIGINAL ARTICLE

A New Method for Activity Monitoring Using Photoplethysmography Signals Recorded by Wireless Sensor

Tugba Aydemir[1] · Mehmet Şahin[1] · Onder Aydemir[2]

Received: 13 July 2020 / Accepted: 5 October 2020 / Published online: 20 October 2020

Abstract

Purpose Different kinds of sensors such as accelerometers and gyroscopes have been used for inferring, predicting, and monitoring human activities for various kinds of applications, including human–computer interaction, surveillance, smart home, health care, and security. In this study, we present a novel and robust method to recognize human activities, including resting, squat, and stepper exercises, solely from photoplethysmography (PPG), which is a non–invasive, simple, and low-cost opto-electronic technique that takes measures from the skin surface.

Methods The features were extracted in raw PPG segments by Hilbert transform and then classified by the *k*-nearest neighbor, naïve Bayes, and decision tree algorithms.

Results The proposed method was successfully applied to the data set recorded from seven subjects and achieved an average classification accuracy rate of 89.39% on the test data. The smaller standard deviation results proved that the proposed method was robust, and the detection of human activities can be effectively performed by Hilbert transform features and decision tree classifier.

Conclusions This PPG-based approach could provide human-activity information in addition to monitoring heart rates and early screenings of various atherosclerotic pathologies, such as cardiovascular and hypertension diseases.

Keywords Photoplethysmography · Activity monitoring · Wireless sensor · Classification

1 Introduction

Photoplethysmography (PPG) is a non-invasive, simple, and low-cost opto-electronic technique that takes measures from the skin surface and can be used to detect blood volume changes in the microvascular bed of tissue [1]. Due to the great potential of widespread clinical application, the PPG technique has been extensively studied in heart rate monitoring [2–4], alcohol consumption [5], and early screening of various atherosclerotic pathologies research, such as cardiovascular and hypertension diseases [6, 7].

In the literature, some studies analyzed PPG signals recorded during various physical activities [8–10]. For example, Zhang et al. proposed a wrist-type PPG signal-based algorithm to combine ensemble empirical mode decomposition with spectrum subtraction for monitoring heart rates during subjects' physical activities, including walking or running on a treadmill. They performed their method on the data set recorded from 12 subjects, achieving an average absolute error of heart rate estimation, i.e., 1.83 beats per minute, with a Pearson correlation of 0.989 between the ground-truth and estimated heart rate [11]. In another PPG-based study, Hwang et al. presented a feasibility analysis of heart rate monitoring of construction workers using a PPG sensor embedded in a wristband-type activity tracker. They recorded the PPG signals from 11 healthy male construction workers (26 to 60 years of age) in masonry, drywall, and electrical operations, which are common in construction. The authors achieved a 4.79% of mean-average percentage error and 0.85 of correlation

✉ Tugba Aydemir
tugba_aydemir17@erdogan.edu.tr

Mehmet Şahin
mehmet.sahin@erdogan.edu.tr

Onder Aydemir
onderaydemir@ktu.edu.tr

[1] Department of Physics, Faculty of Science, Recep Tayyip Erdogan University, 53100 Rize, Turkey

[2] Department of Electrical & Electronics Engineering, Faculty of Engineering, Karadeniz Technical University, 61080 Trabzon, Turkey

coefficient [12]. In another physical-activity-based PPG study, Santos et al. acquired PPG signals from a healthy 28-year-old male volunteer running continuously at speeds of 0, 2, 4, 9, 4, 11, and 0 km/h with a duration of about 2 min each on a treadmill. They approved that their method had potential to monitor cardiac activity at a moderate speed (up to 4 km/h); with increasing speed, however, the motion artifacts dominate the PPG [13].

To the best of our knowledge, this is the second work attempting to recognize physical activities solely from PPG signals. Boukhechba et al. [14] reported that the data set was recorded by wrist-worn smartwatches of 12 participants during five types of activities, including standing, walking, jogging, jumping, and sitting; further, 270 s of PPG signals were acquired for each activity. As a result, they reached an overall F1 score of 0.78. Apart from the above-mentioned study, there is a limited number of papers that recognize human activities from PPG fused with accelerometer signals. For example, Biagetti et al. proposed a human recognition method that classified four physical activity levels, including walking, running, and two resistance levels of biking: low and high. The authors further revealed that, while a classification accuracy (CA) was obtained at around 44.7% using only raw PPG, it achieved 78% by combining PPG with accelerometer signals [15]. On the other hand, some papers recognized human activities using different kinds of methods, including an accelerometer [16, 17], inertial smartphone sensors [18, 19], camera or image-based sensor [20], and the global positioning system [21].

In a human activity recognition-based study, Casale et al. proposed a wearable system that placed an accelerometer on a participant's chest and applied random forest models on 319 manually extracted features from an accelerometer signal to recognize five basic everyday life activities, e.g., walking, climbing stairs, staying standing, talking with people, and working on computer [22]. In an assisted-living-based research, Ma et al. proposed an adaptive-time window-based algorithm of activity recognition. The data were recorded from wheelchair users during sitting, relief, and trunk turning activities by a smart cushion, which was used to detect sitting postures and activities [23]. In another accelerometer-based study, Lu et al. employed an unsupervised method for recognizing physical activities using smartphone accelerometers. They tested their method on a public data set of daily living activities and two data sets of sports activities, i.e., race walking and basketball playing [24]. In a video-based human-activity recognition research, Zhang et al. proposed a Siamese neural network, which alleviated the influence of bad samples generated by conventional data augmentation methods and improved the motion information of videos through input data in human activity recognition systems. The authors tested their method through a video data set, which included 7000 activity videos distributed across 51 action categories with natural disturbances [25].

In line with the previous studies above mentioned, in this study, we contribute to the literature with a novel human activity recognition method, which extracts meaningful features from the PPG to predict resting, squat exercises, and stepper exercises. The features were extracted by Hilbert transform (HT), and they were classified by the *k*-nearest neighbor (*k*-NN), naïve Bayes (NB), and decision tree (DT) classifiers. The proposed method achieved an overall 89.39% of classification accuracy with the DT algorithm. Additionally, to validate its effectiveness we compared the performance of the proposed approach with the band power, wavelet transform (WT) and statistical features.

The remaining sections are organized as follows: in Sect. 2, materials and methods are presented including the data set descriptions, feature extraction, and classification procedure, respectively. Then, the results and performance comparison are provided in tables and a figure in Sect. 3. Finally, Sect. 4 concludes the paper.

2 Materials and Methods

In this section, we first introduce the data set in terms of the types of activities being recognized, the acquisition procedure, and characteristics of the participants. Afterwards, the feature extraction method is described with mathematical equations by expressing the parameter selection procedure. In the last part of this section, the classification stage is presented with the classifier learning method of leave-one-out cross-validation (LOOCV).

2.1 Data Set Description

The data set (available at https://www.ncbi.nlm.nih.gov/pmc/articles/PMC6971339/bin/mmc1.zip) was collected from seven adult healthy subjects (defined as S1, S2,…,S7), which includes three males and four females aged between 20 and 52 years. Detailed written consent was obtained from all participants. The PPG signals were acquired during the voluntary activity from the wrist by using the wireless Maxim Integrated MAXREFDES100 device with a sampling frequency of 400 Hz. In order to provide a tight junction between the sensor and the skin surface, a specific weightlifting cuff has been used, which is adjustable by a tear-off closure with excellent elastic properties. Participants performed five acquisition sessions, each of resting (*class 1*), squat exercises (*class 2*), and stepper exercises (*class 3*). A session loop is given in Fig. 1.

The total recording time (in terms of seconds) for each subject is given in Table 1. The proposed method was tested by splitting the data set into the 1, 2, and 3 s segments

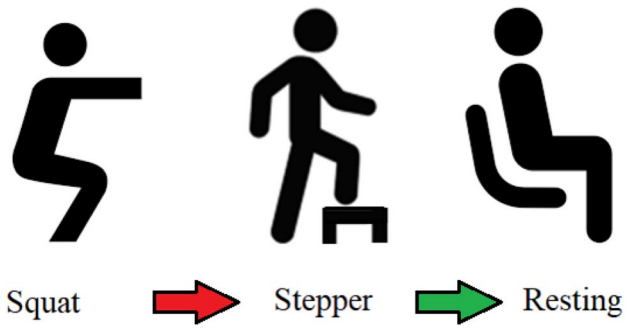

Fig. 1 Session loop in the data-acquisition process

Table 1 Total recording time in seconds

Subject	Squat activity	Stepper activity	Resting activity
S1	311.6	443.0	3271.7
S2	216.8	397.6	2962.8
S3	231.5	271.0	1323.8
S4	212.6	269.7	1361.9
S5	212.6	242.0	1440.9
S6	237.4	325.9	1402.0
S7	266.9	254.9	1510.7

(window lengths) with various overlapping time periods. To illustrate general changes in amplitude patterns, we demonstrate five examples of 3 s recordings for each class in Fig. 2. In this figure, the first, second, and third columns represent resting, squat, and stepper signals, respectively. While the vertical axis represents current in nanoampere (nA), the horizontal axis expresses time in seconds. Table 2 presents the number of obtained segments for each condition. It should be noted that the data splitting procedure was made session by session. Therefore, the last samples of a session, which were not included in a segment, were not added to the next session samples. Note that we randomly selected half of the segments as the training set and the rest of them as the test set. The purpose is to categorize the segments in the test set into *class 1*, *class 2*, or *class 3*.

2.2 Feature Extraction

In this study, the features were extracted by HT, which is a time-domain convolution that maps one real-valued time-history into another [26, 27]. Hence, HT can reveal the local properties of $s(t)$ because the independent variable is not changed in accordance with the transformation. The general formula of HT can be defined by

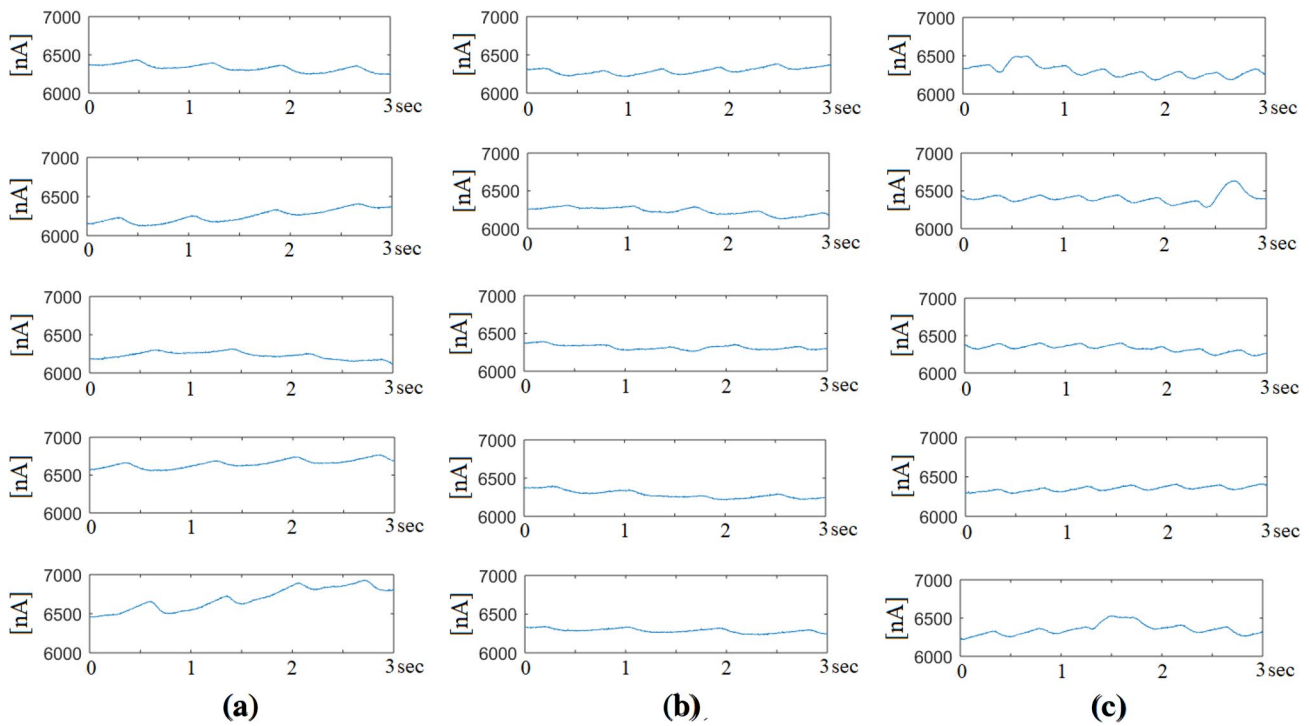

Fig. 2 Examples of 3 s recordings of the raw PPG data: **a** resting, **b** squat, **c** stepper

Table 2 Number of segments for each window length

Activity	Window length											
	1 s			2 s				3 s				
	Overlapping time (S)			Overlapping time (S)				Overlapping Time (S				
	0	0.25	0.5	0	0.25	0.5	1	0	0.25	0.5	1	1.5
Resting												
S1	3268	4358	6535	1633	1866	2177	3263	1089	1187	1304	1630	2174
S2	2960	3946	5918	1478	1690	1970	2955	986	1075	1183	1477	1969
S3	1321	1760	2639	659	752	879	1316	439	479	527	657	874
S4	1360	1813	2717	678	775	904	1355	451	492	541	677	900
S5	1438	1916	2875	718	820	956	1433	478	521	573	715	954
S6	1399	1865	2796	698	797	931	1394	464	507	558	696	927
S7	1509	2010	3014	753	859	1004	1504	500	547	601	751	1000
Squat												
S1	310	411	616	153	175	204	305	101	111	121	152	200
S2	214	284	426	105	120	141	209	70	76	83	104	137
S3	228	304	455	113	130	151	223	75	81	89	110	146
S4	210	279	418	104	118	138	205	68	74	82	101	134
S5	243	323	484	121	138	161	238	80	87	95	117	156
S6	235	313	467	116	132	154	230	76	84	92	114	150
S7	264	352	526	130	149	174	259	86	94	103	129	170
Stepper												
S1	442	586	880	221	249	291	437	146	158	175	216	289
S2	395	527	789	197	224	261	390	130	142	155	193	258
S3	268	357	535	134	151	177	263	88	95	106	129	173
S4	267	356	531	132	151	175	262	87	95	104	130	171
S5	239	318	477	118	135	157	234	78	85	94	116	154
S6	324	430	644	160	182	212	319	107	116	128	159	210
S7	253	335	503	126	143	166	248	83	90	98	122	163

$$\mathrm{H}\{s(t)\} = \frac{1}{\pi}\int_{-\infty}^{\infty}\frac{s(\tau)}{t-\tau}d\tau \tag{1}$$

where t is time, $s(t)$ is a time domain signal, and $\mathrm{H}\{s(t)\}$ is the HT of $s(t)$. Because the output of the HT is, in fact, $\pi/2$ phase shifted version of the original signal $s(t)$, an analytical signal that is associated with the original signal can be constructed as

$$r(t) = p(t) + js(t) = m(t)e^{j\theta(t)} \tag{2}$$

where

$$m(t) = \sqrt{p^2(t) + s^2(t)} \tag{3}$$

and

$$\theta(t) = tan^{-1}\left[\frac{s(t)}{p(t)}\right] \tag{4}$$

where $\theta(t)$ is the instantaneous phase angle. Based on these equations, it is seen that HT produces a complex time series.

In this study, the mean (F1), standard deviation (F2), and autoregressive model parameter (F3) values of the real part and standard deviation (F4) values of the imaginary part were used as features, which were calculated in turn as follows:

$$F1 = \frac{\sum_{i=1}^{N} p(t_i)}{N} \tag{5}$$

$$F2 = \sqrt{\frac{1}{N-1}\sum_{i=1}^{N}\left(p\left(t_i\right) - =p(t)\right)^2} \tag{6}$$

$$F3 = \sum_{i=1}^{b}\beta_i p(t-i) + \epsilon_t \tag{7}$$

$$F4 = \sqrt{\frac{1}{N-1}\sum_{i=1}^{N}(s(t_i) - \overline{S(t)})^2} \tag{8}$$

where N is the length of the real and imaginary parts, β_i ($i=1,2,\ldots,b$) is the b-order autoregressive model coefficients, and ϵ_t is the white noise (independent from the previous points). It is worthwhile mentioning that b presents the order of the autoregressive model, which indicates that current observation depends on b past observations. In this study, we applied a five-order autoregressive model, and $\beta_1, \beta_2, \beta_3, \beta_4, and \beta_5$ were calculated according to Eq. (7), and their absolute values were used as F3 features.

2.3 Classification Procedure

The main goal of the classification stage is sorting the segments in the test set into *class 1*, *class 2*, and *class 3*. In this study, the proposed method is tested by k-NN, NB, and DT classifiers because they are easy to construct and the most commonly used machine learning approaches for classification of PPG signals [15, 16, 23]. Although the k-NN classifier is known as a lazy algorithm, since it does not learn from the training data but simply memorizes the whole training data, it is easy to implement, analytically traceable, and resistant to noisy training set [28]. In the k-NN algorithm, unlabeled test segments are labeled in the training feature space based on the k parameter and the distance measurement technique. In this study, we used the Euclidean metric, which is commonly applied by the machine learning community and achieved better performance. Euclidean distance was calculated as given in Eq. (9):

$$d_e\left(X_i, Y_i\right) = \sqrt{\sum_{i=1}^{n} \left(f_m(X_i) - g_m(Y_i)\right)^2} \tag{9}$$

where m, X_i, and Y_i represent the number of neighbors, the components of vector X and the components of vector Y, respectively. On the other hand, $f_m(X_i)$ and $g_m(Y_i)$ indicate the value of mth neighbor of X_i and the value of mth neighbor of Y_i, respectively. The best k parameter was searched between 1 and 20 by applying the LOOCV technique, which provides one of the best uses of the training data set and avoids the problems of random selections.

We also tested the proposed method by the NB classifier, which is another widely used probabilistic technique. Mostly, it considers a set of training feature space and applies Bayes' theorem with naïve independence assumptions [29]. The NB algorithm probabilistically calculates the class of an unknown segment using the available training feature set to predict the most probable class. The highest probable class F_{NB} of an unknown segment with the conjunction $M=m_1, m_2, \ldots, m_n$ was calculated by

$$F_{NB=\arg \max_{f\varepsilon F} p(f\backslash M)} \tag{10}$$

The DT method is widely used in the machine learning based on the choice of a feature that maximizes classification accuracy and fixes data partition. A DT has one root node for the entire training set, and a new node is added to the DT for every binary partition. Each partition is such that the descendant nodes contain more homogeneous data samples. A partition is chosen because of its ability to render the nodes purer based on a purity measure and can be determined by any single feature. The DT is constructed by training feature space. The rule for tree partition n is based on a node impurity function $f(n)$, which can be calculated as follows:

$$f(n) = \psi(P\left(w_1\backslash n\right), P\left(w_2\backslash n\right), \ldots, P(w_C\backslash n)) \tag{11}$$

where ψ is an arbitrary function and $P(w_j\backslash n)$ represents the probability that a vector Y_t belongs to the class w_j, $j=1,2,\ldots,C$. The measure of the impurity at node n, denoted by $f(n)$, is generally determined by Shannon's information theory as given below:

$$f(n) = -\sum_{j=1}^{C} P\left(w_j\backslash n\right) log_2(P(w_j\backslash n)) \tag{12}$$

where C and log_2 represent the total number of classes and logarithm with base 2, respectively. Each nonterminal node is then split into further binary nodes, n_1 and n_2, such that P_1 and P_2 are the proportions of samples passed to new nodes n_1 and n_2, respectively. The most suitable splitting depends on the maximizing the following difference:

$$\Delta f(n) = f(n) - P_1 f\left(n_1\right) - P_2 f\left(n_2\right) \tag{13}$$

A simple stop-splitting rule has been adopted: If there is no significant decrease in the measure of impurity when a further additional splitting is applied, then splitting is stopped. All these steps are implemented on the training set, and the optimum tree is constructed. Afterward, the features of test segments are classified by the constructed DT model. It should be expressed that the structure of the resulting final tree seems to be rather insensitive to the choice of the partitioning criterion [30].

It should be noticed that the same training procedure was used as applied in the k-NN classifier. On the other hand, we calculated the CA metric to evaluate the performance of the classifiers in terms of percentage (%) as given in Eq. (14). In this equation, R and T indicate the correctly classified PPG segments and the total number of considered segments, respectively:

$$CA = \frac{R}{T} \times 100 \tag{14}$$

The general flowchart of the proposed method is given in Fig. 3. As shown in this figure, we randomly separated the

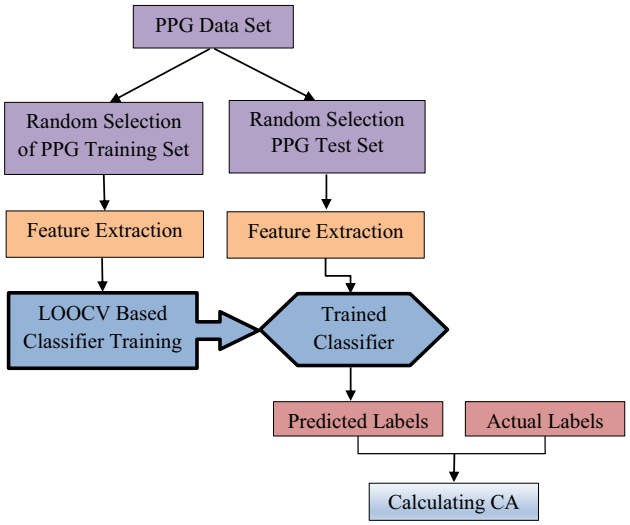

Fig. 3 Flowchart of recognizing human activity system

PPG data set as the training and test sets. It is worthwhile mentioning that the training and test sets include an equal number of segments from each class. Afterward, the features were extracted by the HT. In the training stage, we utilized the LOOCV procedure in order to determine the best k parameter and DT structure. The LOOCV method provided validation of the training set. In this procedure, one trial is removed from the training set, and a new model is fitted using the remaining features of segments. The removed segment is then used to evaluate (cross-validate) the prediction performance of all possible parameters/structures. LOOCV was successively repeated until all the segments were tested. Eventually, we classified test trials based on the trained classifiers. It should be mentioned that the NB does not require a tune parameter in the LOOCV stage. Moreover, we believe that, if certain training and test sets are not given in a public use data set, the proposed method should be performed by many times randomly portioned training and test sets. Hence, in order to avoid the problems of random selections in training and test sets, we applied the demonstrated flowchart procedure 50 times and calculated the average CA metric to robustly evaluate the performance of the classifiers. On the other hand, it should be a remarkable fact that a PPG signal has a non-stationary property and its frequency feature also differs from person to person. Hence, it is reasonable to expect that each subject has one's own dominant timing and HT attributes for extracting discriminative features. Therefore, we trained the classifiers and tested their performance using each person's data individually.

Table 3 Average CA and standard deviation results of 1 s window-length PPG segments

Subject	Classifier	Overlapping time		
		0	0.25	0.5
S1	k-NN	78.29 ± 1.20	78.62 ± 0.81	79.79 ± 0.92
	Bayes	75.16 ± 1.51	75.13 ± 1.21	75.57 ± 1.14
	Tree	82.86 ± 1.43	83.86 ± 1.18	85.16 ± 1.07
S2	k-NN	**99.10 ± 0.40**	99.02 ± 0.32	99.06 ± 0.22
	Bayes	90.96 ± 0.99	91.17 ± 0.91	90.94 ± 0.55
	Tree	98.24 ± 0.67	98.11 ± 0.56	98.49 ± 0.35
S3	k-NN	82.69 ± 1.24	82.52 ± 0.96	82.85 ± 0.85
	Bayes	83.18 ± 1.63	82.90 ± 1.23	83.69 ± 1.17
	Tree	79.51 ± 2.31	79.41 ± 1.65	80.62 ± 1.46
S4	k-NN	97.88 ± 0.51	98.39 ± 0.38	97.88 ± 0.40
	Bayes	95.71 ± 0.93	95.89 ± 0.86	95.70 ± 0.75
	Tree	96.94 ± 0.60	97.47 ± 0.61	97.00 ± 0.54
S5	k-NN	81.86 ± 1.47	83.35 ± 1.36	83.01 ± 1.00
	Bayes	78.30 ± 2.19	76.77 ± 2.20	77.41 ± 1.86
	Tree	84.90 ± 1.68	85.67 ± 1.59	86.24 ± 1.28
S6	k-NN	73.89 ± 1.15	74.50 ± 1.15	74.83 ± 0.91
	Bayes	75.93 ± 1.53	75.49 ± 1.39	76.40 ± 1.00
	Tree	72.13 ± 2.16	73.47 ± 1.58	73.70 ± 1.41
S7	k-NN	82.63 ± 1.18	80.50 ± 1.52	81.59 ± 0.99
	Bayes	82.87 ± 1.24	87.61 ± 1.12	87.45 ± 0.93
	Tree	80.14 ± 1.45	86.01 ± 1.33	86.29 ± 1.27
Avg	k-NN	85.19 ± 1.02	85.28 ± 0.93	85.58 ± 0.76
	Bayes	83.16 ± 1.43	83.57 ± 1.28	83.89 ± 1.06
	Tree	84.96 ± 1.47	86.29 ± 1.22	**86.79 ± 1.06**

3 Results

In this study, we present a novel and robust method to recognize human activities, including resting, squat, and stepper exercises solely from 1, 2, and 3 s window-length PPG segments. The window lengths were considered with nonoverlapping and various overlapping time periods. While the features were extracted from those segments by calculating the statistical and autoregressive model parameter values of HT, they were tested by the k-NN, NB, and DT classifiers. As noted, in order to show the robustness, the proposed method was run 50 times, which means that, in every run, we randomly split the training and test sets and calculate an average CA and a standard deviation value for all runs. The CA and standard deviation results for 1, 2, and 3 s window-length PPG segments are given in Tables 3, 4, and 5, respectively. In these tables, the best average and classifier performances are highlighted in bold. Although there was not a significant difference among the classifiers, the DT algorithm has higher CA results on average for each window length. It can be also seen from Table 3 that, while the highest CA was achieved by k-NN as 99.10% ± 0.40 for S2

Table 4 Average CA and standard deviation results of 2 s window-length PPG segments

Subject	Classifier	Overlapping time			
		0	0.25	0.5	1
S1	*k*-NN	77.85 ± 1.13	78.08 ± 1.40	78.72 ± 1.30	79.26 ± 1.26
	Bayes	77.71 ± 1.82	76.81 ± 1.59	77.48 ± 1.78	78.10 ± 1.19
	Tree	83.00 ± 1.73	83.41 ± 2.01	84.16 ± 1.79	84.82 ± 1.59
S2	*k*-NN	99.04 ± 0.49	99.16 ± 0.48	99.08 ± 0.43	**99.15 ± 0.35**
	Bayes	91.20 ± 1.26	91.12 ± 1.48	91.05 ± 1.41	90.98 ± 1.30
	Tree	98.15 ± 0.77	98.65 ± 0.50	98.28 ± 0.57	98.07 ± 0.72
S3	*k*-NN	83.10 ± 2.18	84.14 ± 1.69	82.55 ± 1.53	83.68 ± 1.30
	Bayes	84.38 ± 2.02	83.92 ± 1.67	82.40 ± 1.93	83.79 ± 1.58
	Tree	81.02 ± 2.43	81.59 ± 2.52	80.97 ± 2.18	82.87 ± 1.77
S4	*k*-NN	97.89 ± 0.80	98.16 ± 0.72	98.36 ± 0.63	98.25 ± 0.58
	Bayes	94.98 ± 1.46	95.90 ± 1.30	95.73 ± 1.43	96.03 ± 1.11
	Tree	96.85 ± 1.16	97.72 ± 1.05	97.74 ± 0.58	98.07 ± 0.61
S5	*k*-NN	81.74 ± 2.31	82.19 ± 1.87	82.58 ± 1.63	81.51 ± 1.28
	Bayes	81.36 ± 2.66	81.97 ± 3.01	81.10 ± 2.50	81.74 ± 1.86
	Tree	86.64 ± 2.03	87.25 ± 1.77	87.33 ± 2.22	88.99 ± 2.04
S6	*k*-NN	77.66 ± 1.75	76.99 ± 1.85	78.03 ± 1.46	78.65 ± 1.36
	Bayes	79.20 ± 1.86	79.80 ± 2.17	80.31 ± 1.79	80.09 ± 1.27
	Tree	74.89 ± 2.79	74.52 ± 2.36	75.96 ± 2.51	76.59 ± 1.82
S7	*k*-NN	75.20 ± 2.63	75.19 ± 2.15	75.49 ± 1.99	76.57 ± 1.60
	Bayes	87.71 ± 1.46	88.66 ± 1.70	88.25 ± 1.58	88.83 ± 1.35
	Tree	85.60 ± 2.41	86.23 ± 2.10	85.96 ± 1.88	86.68 ± 1.65
Avg	*k*-NN	84.64 ± 1.61	84.84 ± 1.45	84.97 ± 1.28	85.29 ± 1.11
	Bayes	85.22 ± 1.79	85.45 ± 1.84	85.18 ± 1.78	85.65 ± 1.38
	Tree	86.59 ± 1.90	87.05 ± 1.75	87.20 ± 1.68	**88.01 ± 1.46**

when the overlapping time was 0 s, the lowest performance was obtained by DT as 72.13% for S6 with 1 s window-length PPG segments. Moreover, the best average CA of all subjects was achieved by the DT classifier as 86.79% ± 1.06 when the overlapping time was 0.5 s. It is worthwhile to note that we tested 0, 0.25, and 0.5 s overlapping time periods for PPG segments. However, there was also not a significant difference among the overlapping time periods in terms of CA and standard deviation.

In the results of 2 s window-length PPG segments, the best CA was achieved by the DT classifier for S2 as 99.15% ± 0.35 when the overlapping time was 1 s. Contrary to this, the worst performance was calculated by the NB for S6 as 74.52% when the overlapping time was 0.25 s. Additionally, the highest average CA of all subjects was again achieved by the DT classifier as 88.01% ± 1.46 when the overlapping time was 1 s.

In the results of 3 s window-length PPG segments, the best CA was achieved by the *k*-NN classifier for S2 as 99.62% ± 0.36 when the overlapping time was 0 s. Contrary to this, the worst performance was calculated by the *k*-NN for S7 as 73.27% when the overlapping time was 0 s. Additionally, the highest average CA of all subjects was again achieved by the DT classifier as 89.39% ± 1.62 when the overlapping time was 1.5 s. Based on the smaller standard deviation values, it can be expressed that the proposed method was robust and stable.

In this research, the proposed approach was compared with the band power, WT, and statistical features, which are commonly used in biomedical pattern-recognition-based applications. While 0–50 Hz band power [31, 32] was calculated for the band power feature, a Morlet mother wavelet with 1 to 50 scale range (with integer interval) was used to obtain WT [33, 34] coefficients. The WT features were obtained by calculating the standard deviation and average values of WT coefficients. We calculated kurtosis, skewness, variance, and sum of derivative values for the statistical features [34]. It should be noted that the same training procedure was used as applied in the proposed method. The performance comparison was tested in terms of CA, and the results, which were calculated for 3 s window-length PPG segments with 1.5 s overlapping time, are given in Fig. 4. In this figure, the vertical lines on top of the bars represent standard deviations. The highest classification accuracies were achieved as 81.61%, 81.67%, and 60.42% for band power, WT, and statistical features, respectively. The results showed that the HT-based

Table 5 Average CA and standard deviation results of 3 s window-length PPG segments

Subject	Classifier	Overlapping time				
		0	0.25	0.5	1	1.5
S1	*k*-NN	79.40 ± 1.77	80.83 ± 2.14	79.45 ± 1.45	80.08 ± 1.47	80.82 ± 1.22
	Bayes	77.79 ± 2.28	77.06 ± 2.33	78.16 ± 2.21	78.95 ± 1.90	78.68 ± 1.31
	Tree	82.63 ± 2.75	83.33 ± 2.84	85.01 ± 2.26	84.52 ± 2.81	86.23 ± 1.91
S2	*k*-NN	**99.62 ± 0.36**	99.32 ± 0.64	99.36 ± 0.36	99.55 ± 0.55	99.50 ± 0.32
	Bayes	91.61 ± 1.78	91.44 ± 2.10	91.28 ± 1.28	91.60 ± 1.35	91.55 ± 1.28
	Tree	98.60 ± 1.32	99.21 ± 0.72	98.88 ± 0.64	98.78 ± 0.76	99.16 ± 0.56
S3	*k*-NN	82.17 ± 2.70	83.43 ± 1.92	83.88 ± 2.10	85.08 ± 1.78	84.71 ± 1.46
	Bayes	83.95 ± 2.92	83.78 ± 2.45	84.18 ± 2.52	83.29 ± 2.25	83.95 ± 1.74
	Tree	79.68 ± 3.34	82.18 ± 3.83	82.07 ± 2.82	83.61 ± 2.53	83.70 ± 2.17
S4	*k*-NN	98.55 ± 0.76	98.63 ± 0.85	98.31 ± 0.77	98.55 ± 0.85	98.76 ± 0.49
	Bayes	96.70 ± 1.63	95.48 ± 2.08	94.96 ± 2.03	96.86 ± 1.52	96.79 ± 1.19
	Tree	98.01 ± 1.48	98.43 ± 1.16	97.93 ± 1.16	97.84 ± 1.22	98.26 ± 0.91
S5	*k*-NN	82.86 ± 2.21	83.20 ± 2.42	81.64 ± 2.46	82.05 ± 1.88	82.58 ± 1.57
	Bayes	80.91 ± 3.47	82.47 ± 2.62	83.43 ± 2.89	82.28 ± 2.67	82.76 ± 2.73
	Tree	88.44 ± 3.13	87.41 ± 3.53	86.64 ± 3.29	89.74 ± 2.55	90.66 ± 1.89
S6	*k*-NN	82.38 ± 2.25	79.30 ± 2.24	79.87 ± 2.12	80.88 ± 1.81	81.68 ± 1.66
	Bayes	83.24 ± 2.11	82.94 ± 2.48	81.85 ± 2.32	83.38 ± 2.07	82.24 ± 1.61
	Tree	77.47 ± 4.01	77.68 ± 3.13	77.41 ± 2.45	78.09 ± 2.94	79.77 ± 2.18
S7	*k*-NN	73.27 ± 2.44	74.26 ± 2.57	74.34 ± 2.54	73.81 ± 2.12	74.65 ± 1.89
	Bayes	89.19 ± 2.09	88.42 ± 2.39	86.68 ± 1.94	88.78 ± 1.63	89.63 ± 1.86
	Tree	85.84 ± 2.67	86.99 ± 2.36	85.96 ± 2.47	87.28 ± 2.32	87.93 ± 1.73
Avg	*k*-NN	85.46 ± 1.78	85.56 ± 1.83	85.27 ± 1.69	85.71 ± 1.49	86.10 ± 1.23
	Bayes	86.20 ± 2.32	85.94 ± 2.35	85.79 ± 2.17	86.45 ± 1.91	86.52 ± 1.67
	Tree	87.24 ± 2.67	87.89 ± 2.51	87.70 ± 2.16	88.55 ± 2.16	**89.39 ± 1.62**

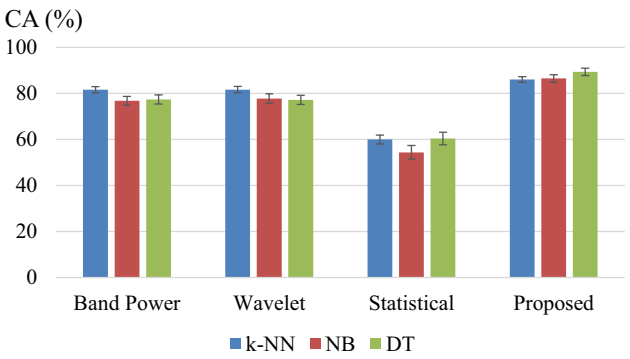

Fig. 4 Performance comparison

human-activity recognition method was 7.72% higher than the best CA result of compared methods.

4 Conclusion

In this study, a novel human activity recognition method has been successfully applied to the PPG data set recorded from seven subjects. The proposed method allows extraction of discriminative features by calculating statistical and autoregressive model parameters of HT. It is noteworthy that we achieved the average CA rate of 89.39% for 3 s PPG signal segments. It should also be emphasized that the maximum performance was achieved more than 99% for S2 in every window-length.

In order to show its capacity, we compared the proposed method with the mostly used feature extraction algorithms, where our method provided an improvement of 7.72%. The smaller standard deviation values proved that the proposed method was robust and stable. Consequently, we believe that the proposed method can be successfully applied to PPG signals for human-activity recognition.

It should be mentioned that the goal of this work was not to replace the widely used motion sensors but to present an alternative way on how PPG signals could be leveraged in human-activity recognition. For instance, the PPG-based approach could be used to monitor human activities when gyroscopes or other sensors are not available. In addition to monitoring heart rates and early screenings of various atherosclerotic pathologies, such as cardiovascular and hypertension diseases, this approach could also provide human-activity information. Moreover, the successful results showed that PPG signals could also be used

in hybrid approaches with other sensors to enhance the recognition accuracy.

Compliance with Ethical Standards

Conflict of interest There is not any conflict of interest.

References

1. Allen, J. (2007). Photoplethysmography and its application in clinical physiological measurement. *Physiological Measurement, 28*(3), R1.
2. Zhang, Z., Pi, Z., & Liu, B. (2014). TROIKA: A general framework for heart rate monitoring using wrist-type photoplethysmographic signals during intensive physical exercise. *IEEE Transactions on Biomedical Engineering, 62*(2), 522–531.
3. Zhao, D., Sun, Y., Wan, S., & Wang, F. (2017). SFST: A robust framework for heart rate monitoring from photoplethysmography signals during physical activities. *Biomedical Signal Processing and Control, 33,* 316–324.
4. Prabhakar, S. K., Rajaguru, H., & Lee, S. W. (2019). Metaheuristic-based dimensionality reduction and classification analysis of PPG signals for interpreting cardiovascular disease. *IEEE Access, 7,* 165181–165206.
5. Wang, W. F., Yang, C. Y., & Wu, Y. F. (2018). SVM-based classification method to identify alcohol consumption using ECG and PPG monitoring. *Personal and Ubiquitous Computing, 22*(2), 275–287.
6. Yang, C., Veiga, C., Rodríguez-Andina, J. J., Farina, J., Iniguez, A., & Yin, S. (2019). Using PPG signals and wearable devices for atrial fibrillation screening. *IEEE Transactions on Industrial Electronics, 66*(11), 8832–8842.
7. Liang, Y., Chen, Z., Ward, R., & Elgendi, M. (2018). Photoplethysmography and deep learning: enhancing hypertension risk stratification. *Biosensors, 8*(4), 101.
8. Casson, A. J., Galvez, A. V., & Jarchi, D. (2016). Gyroscope vs accelerometer measurements of motion from wrist PPG during physical exercise. *ICT Express, 2*(4), 175–179.
9. Stahl, S. E., An, H. S., Dinkel, D. M., Noble, J. M., & Lee, J. M. (2016). How accurate are the wrist-based heart rate monitors during walking and running activities? Are they accurate enough? *BMJ Open Sport & Exercise Medicine, 2*(1), e000106.
10. Jarchi, D., & Casson, A. J. (2017). Towards photoplethysmography-based estimation of instantaneous heart rate during physical activity. *IEEE Transactions on Biomedical Engineering, 64*(9), 2042–2053.
11. Zhang, Y., Liu, B., & Zhang, Z. (2015). Combining ensemble empirical mode decomposition with spectrum subtraction technique for heart rate monitoring using wrist-type photoplethysmography. *Biomedical Signal Processing and Control, 21,* 119–125.
12. Hwang, S., Seo, J., Jebelli, H., & Lee, S. (2016). Feasibility analysis of heart rate monitoring of construction workers using a photoplethysmography (PPG) sensor embedded in a wristband-type activity tracker. *Automation in Construction, 71,* 372–381.
13. Santos, S. A., Venema, B., & Leonhardt, S. (2012). Accelerometer-assisted PPG measurement during physical exercise using the LAVIMO sensor system. *Acta Polytechnica, 52*(5), 80–85.
14. Boukhechba, M., Cai, L., Wu, C., & Barnes, L. E. (2019). ActiPPG: Using deep neural networks for activity recognition from wrist-worn photoplethysmography (PPG) sensors. *Smart Health, 14,* 100082.
15. Biagetti, G., Crippa, P., Falaschetti, L., Orcioni, S., & Turchetti, C. (2017). Human activity recognition using accelerometer and photoplethysmographic signals. In *International Conference on Intelligent Decision Technologies*, (pp. 53–62). Springer, Cham.
16. Attal, F., Mohammed, S., Dedabrishvili, M., Chamroukhi, F., Oukhellou, L., & Amirat, Y. (2015). Physical human activity recognition using wearable sensors. *Sensors, 15*(12), 31314–31338.
17. Khan, A. M., Lee, Y. K., Lee, S. Y., & Kim, T. S. (2010). A triaxial accelerometer-based physical-activity recognition via augmented-signal features and a hierarchical recognizer. *IEEE Transactions on Information Technology in Biomedicine, 14*(5), 1166–1172.
18. Hassan, M. M., Uddin, M. Z., Mohamed, A., & Almogren, A. (2018). A robust human activity recognition system using smartphone sensors and deep learning. *Future Generation Computer Systems, 81,* 307–313.
19. Reyes-Ortiz, J. L., Oneto, L., Samà, A., Parra, X., & Anguita, D. (2016). Transition-aware human activity recognition using smartphones. *Neurocomputing, 171,* 754–767.
20. Chen, L., Wei, H., & Ferryman, J. (2013). A survey of human motion analysis using depth imagery. *Pattern Recognition Letters, 34*(15), 1995–2006.
21. Boukhechba, M., Chow, P., Fua, K., Teachman, B. A., & Barnes, L. E. (2018). Predicting social anxiety from global positioning system traces of college students: feasibility study. *JMIR Mental Health, 5*(3), e10101.
22. Casale, P., Pujol, O., & Radeva, P. (2011). Human activity recognition from accelerometer data using a wearable device. In *Iberian Conference on Pattern Recognition and Image Analysis* (pp. 289–296).
23. Ma, C., Li, W., Cao, J., Du, J., Li, Q., & Gravina, R. (2020). Adaptive sliding window based activity recognition for assisted livings. *Information Fusion, 53,* 55–65.
24. Lu, Y., Wei, Y., Liu, L., Zhong, J., Sun, L., & Liu, Y. (2017). Towards unsupervised physical activity recognition using smartphone accelerometers. *Multimedia Tools and Applications, 76*(8), 10701–10719.
25. Zhang, Y., Po, L. m., liu, m., rehman, y. a. u., ou, w., & zhao, y. (2020). data-level information enhancement: Motion-patch-based siamese convolutional neural networks for human activity recognition in Videos. *Expert Systems with Applications*, 113203.
26. Peng, Z. K., Peter, W. T., & Chu, F. L. (2005). An improved Hilbert-Huang transform and its application in vibration signal analysis. *Journal of Sound and Vibration, 286*(1–2), 187–205.
27. Sahoo, S., Biswal, P., Das, T., & Sabut, S. (2016). De-noising of ECG signal and QRS detection using Hilbert transform and adaptive thresholding. *Procedia Technology, 25,* 68–75.
28. Wettschereck, D., Aha, D. W., & Mohri, T. (1997). A review and empirical evaluation of feature weighting methods for a class of lazy learning algorithms. *Artificial Intelligence Review, 11*(1–5), 273–314.
29. Gupta, N., Ahuja, N., Malhotra, S., Bala, A., & Kaur, G. (2017). Intelligent heart disease prediction in cloud environment through ensembling. *Expert Systems*. 34(3), Article Number: e12207.
30. Breiman, L., Friedman, J., Stone, C. J., & Olshen, R. A. (1984). *Classification and regression trees*. Boca Raton: CRC Press.
31. Parvinnia, E., Sabeti, M., Jahromi, M. Z., & Boostani, R. (2014). Classification of EEG Signals using adaptive weighted distance nearest neighbor algorithm. *Journal of King Saud University-Computer and Information Sciences, 26*(1), 1–6.
32. Aydemir, O. (2017). Olfactory recognition based on eeg gamma-band activity. *Neural Computation, 29*(6), 1667–1680.
33. Karimian, N., Guo, Z., Tehranipoor, M., & Forte, D. (2017, March). Human recognition from photoplethysmography (ppg) based on non-fiducial features. In *2017 IEEE International Conference on Acoustics, Speech and Signal Processing*, pp. 4636–4640.
34. Jegadeeshwaran, R., & Sugumaran, V. (2015). Fault diagnosis of automobile hydraulic brake system using statistical features and support vector machines. *Mechanical Systems and Signal Processing, 52,* 436–446.